Turkish Journal of Electrical Engineering & Computer Sciences

http://journals.tubitak.gov.tr/elektrik/

Research Article

Turk J Elec Eng & Comp Sci
(2019) 27: 2998 – 3014

doi:10.3906/elk-1809-166

A control scheme for maximizing the delivered power to the load in a standalone wind energy conversion system

Saeed HESHMATIAN, Davood ARAB KHABURI*, Mahyar KHOSRAVI, Ahad KAZEMI
Department of Electrical Engineering, Iran University of Science and Technology, Tehran, Iran

Received: 23.09.2018 • **Accepted/Published Online:** 31.03.2019 • **Final Version:** 26.07.2019

Abstract: In this paper, a control scheme is proposed for maximum power point tracking (MPPT) in a variable speed standalone wind energy conversion system (WECS) with permanent magnet synchronous generator. A MPPT algorithm is designed trying to eliminate the main deficiency of the conventional perturbation and observation (P&O) method, which is the challenge of choosing a proper step size and the unwanted trade-off between accuracy and speed. The designed algorithm properly addresses this drawback and significantly improves the MPPT performance. Another important issue is to ensure fast and accurate tracking of the optimal reference point obtained from the MPPT algorithm and improve the performance and efficiency of the control system for transferring maximum possible power to the load. To this end, a Vienna rectifier is used in the designed WECS and a multiobjective model predictive control scheme is designed to properly control the converter with fast response, high accuracy, and, at the same time, the lowest possible switching frequency. The performance of the proposed control scheme has been studied for two different wind speed profiles with different behaviors. Moreover, a comparison is made between the proposed MPPT algorithm and the conventional P&O method. The results support the proper performance of the proposed system in extraction and transfer of the maximum possible power from the wind to the load. This aim is achieved because of the significant advantages of the designed system in terms of fast and accurate tracking of the optimal point and having higher efficiency.

Key words: Maximum power point tracking, multiobjective model predictive control, wind energy conversion system, switching frequency reduction, Vienna rectifier

1. Introduction

There are various forms of renewable energy resources and wind energy is undoubtedly among the most important and promising ones. In addition to the wind turbine and the electrical generator, which are the main parts, a proper converter interface and its control system are also necessary in a wind energy conversion system (WECS). The permanent magnet synchronous generator (PMSG) is the dominant technology in these systems due to its notable advantages such as high efficiency and high power density, good reliability, and low maintenance [1, 2]. A power electronic interface is required for connecting a WECS to the electrical load or power network. This interface mainly consists of a rectifier and an inverter, which are called the generator- and grid-side converters, respectively.

A classical six-switch rectifier is widely used as the generator-side converter in WECSs because of its simplicity. However, this converter does not provide satisfactory performance and has some major drawbacks such as high harmonic distortion and low efficiency. In this work, a Vienna rectifier is utilized in the studied

*Correspondence: khaburi@iust.ac.ir

WECS in order to improve the performance of the system. This topology was introduced for being utilized in power supply devices used in communication systems in 1997 [3]. The Vienna rectifier has important features that makes it preferable for use as the generator-side converter in a WECS. The harmonic distortion in the AC side of this converter is relatively lower and also the power factor is close to unity. The switching scheme is much simpler and the converter has lower cost and higher efficiency because there are just three active switches in the structure and the voltage stress imposed on those switches is small [4]. Moreover, it does not have dead time and is capable of high frequency operation. The power flow in this converter is unidirectional and therefore it is not suitable for many applications in which the power flow is required in both directions. However, the power flow in wind energy conversion is unidirectional from the AC side to the load; therefore, Vienna topology is an advantageous choice for this application.

Model predictive control (MPC) is one of the most advantageous methods for controlling power electronic converters. The basic principle of this method is to utilize an appropriate model of the system to predict the future behavior of a control variable until a predefined horizon in time. This information is used by the controller to determine the next optimal actuation based on minimizing a predefined cost function. This method has some notable advantages: the concepts are simple and easy to understand and implement. The multivariable case can be easily considered and the nonlinearities can be included into the model. Moreover, the dead times can be compensated and the constraints can be easily treated [5].

The most important reason to control the machine-side converter is to maximize the captured energy from the wind. The main conventional maximum power point tracking (MPPT) methods employed in wind energy conversion are tip speed ratio (TSR), optimal torque control (OTC), power signal feedback (PSF), and perturbation and observation (P&O), also known as hill-climbing search (HSC) [6, 7]. In the TSR algorithm, the rotational speed reference is determined by keeping the tip speed ratio at its optimal value [8, 9]. Although this method is simple and fast, it is not accurate enough in tracking the maximum power point. Moreover, this method requires measurement of the effective wind speed, which is costly, inaccurate, and difficult to accomplish [7]. The OTC method adjusts the generator torque to its optimal value obtained from the optimum torque-speed curve of the system [1, 8]. The PSF method has a similar principle to the OTC algorithm. In this method, the optimal power-speed curve is used as a look-up table or a mathematical expression in order to determine the optimal power reference required for tracking the maximum power point [10]. The PSF and OTC methods do not need wind speed measurements but do require knowledge of system parameters and air density, and they are highly dependent on these parametric values and will be affected by changes in these parameters. Optimal characteristic curves are also required, which will change as the system ages [6, 11].

The P&O search algorithm is widely utilized in order to implement MPPT in WECSs [12, 13]. This algorithm is simple since prior knowledge of the parametric values or wind speed measurements is not required [1, 7]. However, it has one main drawback, which lies in the challenge of choosing the right perturbation step size. The P&O algorithm with small step size is slow in tracking the MPP, especially in rapid wind variations. On the other hand, by increasing the step size to make the method faster, there will be unwanted oscillations around the maximum point and the MPPT accuracy and efficiency will be reduced [6, 14]. The two-step-value HCS algorithm was proposed in [15, 16] in order to improve the performance of this method. Variable step size has also been considered to overcome the aforementioned conflicting problem of the conventional HCS method [17]. These methods improve the performance of the HCS algorithm, but they do not completely present satisfactory performance, especially in rapidly varying wind speeds. In addition to the aforementioned MPPT

algorithms, some other methods have been proposed in the literature. Fuzzy logic control has been employed for implementing variable-speed HCS algorithms [18, 19]. Some efforts have been made in order to use neural networks for realization of MPPT in WECSs [20, 21]. Sliding mode control (SMC) was also applied to WECSs in [19, 22] for maximizing the captured energy.

In this paper, a control structure is proposed for a standalone WECS. This control scheme includes an improved MPPT algorithm, which eliminates the aforementioned problems of the P&O method in the case of tracking the optimum point. Also, the system is designed based on a Vienna rectifier because of its high efficiency and good performance, and it is controlled by a multiobjective MPC strategy for fast and accurate tracking of the optimal reference point obtained from the MPPT algorithm. A secondary control objective is considered in the cost function in order to limit the switching frequency and hence reduce the power losses. The proposed control scheme shows great performance and is advantageous compared to conventional approaches in terms of extracting the maximum possible power and transferring it to the load by providing fast and accurate response, especially for wind speed profiles with fast variations.

2. System configuration and modeling

Figure 1 shows the overall configuration of the studied WECS with the designed control scheme. In this section, modeling and analysis of the main parts are presented.

2.1. Wind turbine modeling

The mechanical output power for a variable-speed wind turbine is given by the following expression:

$$P_m = \frac{1}{2} c_p \rho A V_w^3, \tag{1}$$

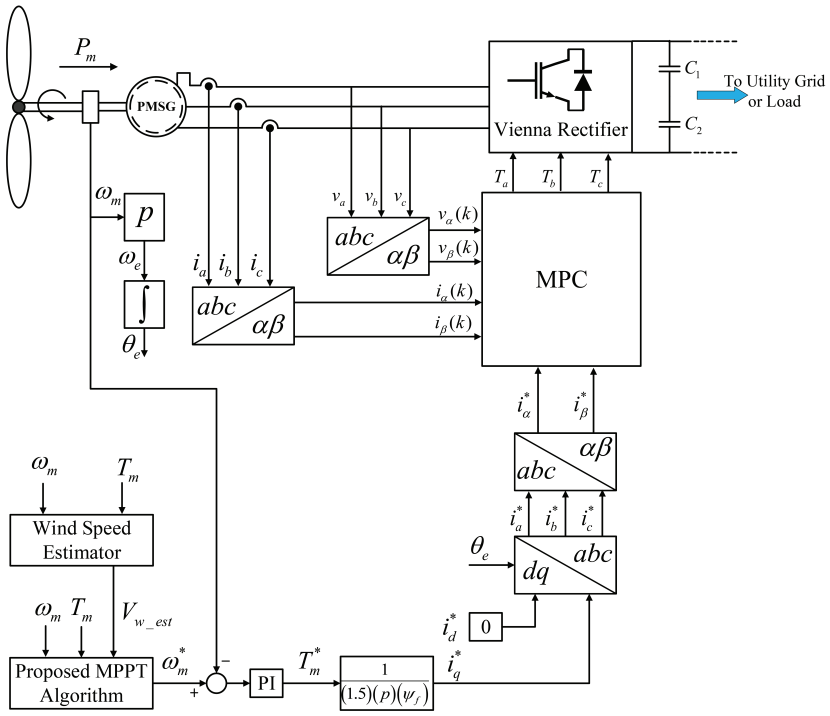

Figure 1. Studied WECS.

where P_m is the mechanical power, V_w is the wind speed, and ρ represents the air density. A is the swept area by the blades and is given by $A = \pi R^2$, where R is the radius of the blades. c_p represents the power coefficient and is described by a nonlinear function of the blade's pitch angle (β) and the tip speed ratio (λ) as expressed in Eqs. (2) and (3) [23]. The ratio between the linear velocity of the tip of the blades and the effective wind speed around them is called the tip speed ratio and is given in Eq. (4). Table 1 shows the coefficients in Eq. (2).

$$c_p(\lambda,\beta) = k_1\left(k_2\frac{1}{\lambda_i} - k_3\beta - k_4\right)e^{\left(-k_5\frac{1}{\lambda_i}\right)} + k_6\lambda, \tag{2}$$

$$\frac{1}{\lambda_i} = \frac{1}{\lambda + 0.08\beta} - \frac{0.035}{1+\beta^3}, \tag{3}$$

$$\lambda = \frac{R.\omega_m}{V_w}, \tag{4}$$

where ω_m is the mechanical angular speed. The $c_p - \lambda$ curves for the studied wind turbine are depicted in Figure 2 for different pitch angle values. As is obvious from this figure, the curve corresponding to $\beta = 0$ has the highest peak value, which occurs at $\lambda_{opt} = 8.1$ and is equal to $c_{p_{max}} = 0.48$. In a typical WECS, when the wind speed goes beyond the nominal value, the pitch angle control is required to limit the mechanical power and to ensure system safety. However, the concentration of this paper is on the MPPT and it is assumed that the wind speed does not exceed the nominal value. Therefore, the pitch angle of the studied turbine is assumed to be fixed at $\beta = 0$ and Eq. (2) is approximated based on this assumption as expressed in Eq. (5):

$$c_p(\lambda) = \sum_{i=0}^{5} a_i\lambda^i = a_0 + a_1\lambda + a_2\lambda^2 + a_3\lambda^3 + a_4\lambda^4 + a_5\lambda^5. \tag{5}$$

Table 1 shows the coefficients in Eq. (5). The mechanical equation of torque and speed is expressed in Eq. (6), where T_e is the generator electromagnetic torque and T_m is the wind turbine mechanical torque. F and J represent the rotor friction factor and the total inertia, respectively:

$$J\frac{d\omega_m}{dt} = T_m - T_e - F\omega_m, \tag{6}$$

Table 1. Values of the coefficients in c_p equations.

k_i	Value	a_i	Value
k_1	0.5176	a_0	0.15006
k_2	116	a_1	-0.17732
k_3	0.4	a_2	0.058833
k_4	0.5	a_3	-28.083×10^{-4}
k_5	21	a_4	-28.35×10^{-5}
k_6	0.0068	a_5	1.7864×10^{-5}

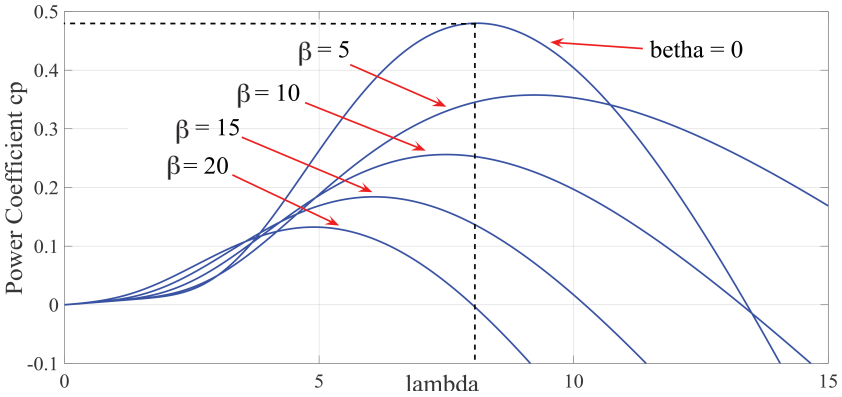

Figure 2. Power coefficient curves for different values of pitch angle.

2.2. PMSG modeling

The PMSG can be modeled in the direct-quadrature (dq) synchronous reference frame in the following form [24]:

$$\begin{bmatrix} v_{sd} \\ v_{sq} \end{bmatrix} = R_s \begin{bmatrix} i_{sd} \\ i_{sq} \end{bmatrix} + \frac{d}{dt} \begin{bmatrix} \Psi_{sd} \\ \Psi_{sq} \end{bmatrix} + \omega_e \begin{bmatrix} 0 & -1 \\ 1 & 0 \end{bmatrix} \begin{bmatrix} \Psi_{sd} \\ \Psi_{sq} \end{bmatrix}, \tag{7}$$

where v_{sd}, v_{sq}, i_{sd}, i_{sq}, Ψ_{sd}, and Ψ_{sq} represent direct and quadrature components of the stator voltage, current, and flux, respectively. R_s is the resistance of the stator winding and ω_e is the electrical angular speed, which is related to the mechanical angular rotational speed (ω_m) by the equation $\omega_e = p\omega_m$ where p is the number of generator pole pairs. By assuming that the d-axis of the synchronously rotating reference frame is aligned along the rotor flux direction, the stator flux components can be given as:

$$\begin{bmatrix} \Psi_{sd} \\ \Psi_{sq} \end{bmatrix} = \begin{bmatrix} L_{sd} & 0 \\ 0 & L_{sq} \end{bmatrix} \begin{bmatrix} i_{sd} \\ i_{sq} \end{bmatrix} + \begin{bmatrix} \Psi_f \\ 0 \end{bmatrix}, \tag{8}$$

where L_{sd} and L_{sq} are d- and q-axis inductances, respectively. Ψ_f represents the amplitude of the flux linkage established by the permanent magnet. By substituting Eq. (8) into Eq. (7), the following expression is obtained for generator voltages:

$$\begin{bmatrix} v_{sd} \\ v_{sq} \end{bmatrix} = R_s \begin{bmatrix} i_{sd} \\ i_{sq} \end{bmatrix} + \frac{d}{dt} \begin{bmatrix} L_{sd} i_{sd} \\ L_{sq} i_{sq} \end{bmatrix} + \omega_e \begin{bmatrix} -L_{sq} i_{sq} \\ L_{sd} i_{sd} + \Psi_f \end{bmatrix}. \tag{9}$$

By considering Eq. (8), the electromagnetic torque developed by the generator is expressed as in the following equation:

$$T_e = \frac{3}{2} p(\Psi_{sd} i_{sq} - \Psi_{sq} i_{sd}) = \frac{3}{2} p\left(\Psi_f i_{sq} + (L_{sd} - L_{sq}) i_{sd} i_{sq}\right). \tag{10}$$

The PMSG used in the studied system is assumed to have a cylindrical rotor in which L_{sd} and L_{sq} are equal. Therefore, the electromagnetic torque in Eq. (10) is simplified as:

$$T_e = \frac{3}{2} p \Psi_f i_{sq}. \tag{11}$$

It can be concluded from Eq. (11) that control of the electromagnetic torque and hence the rotational speed can be done by adjusting i_{sq}. Figure 3 shows the equivalent circuits of the PMSG in the d- and q-axes.

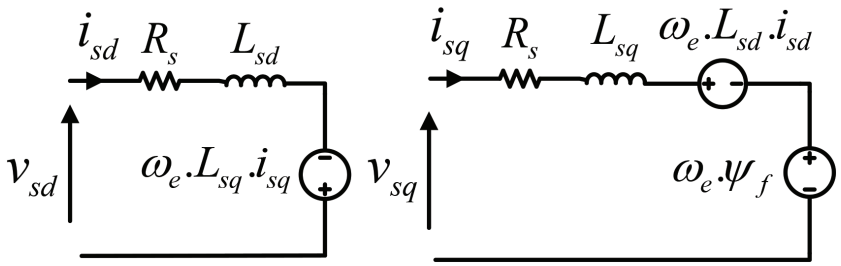

Figure 3. Equivalent circuits of PMSG in d- and q-axes.

2.3. Vienna rectifier modeling

Figure 4 depicts the Vienna rectifier with three-phase structure. Applying Kirchhoff's voltage law to this topology yields the following equation:

$$V_{sabc} = L_s \frac{di_{abc}}{dt} + R_s i_{abc} + v_{rabcN} - v_{nN}, \tag{12}$$

where V_{sabc} and i_{abc} are source voltages and phase currents, respectively. v_{rabcN} and v_{nN} represent the voltage difference of the points r_{abc} and the neutral point n in relation to the DC center point (N), respectively. The vector form of Eq. (12) is given in the following equations:

$$\overline{\mathbf{V_s}} = L_s \frac{d}{dt}(\overline{\mathbf{I_s}}) + R_s(\overline{\mathbf{I_s}}) + \overline{\mathbf{V_{rN}}} - \overline{\mathbf{V_{nN}}}, \tag{13}$$

$$\overline{\mathbf{V_s}} = \frac{2}{3}\left(v_{sa} + \alpha v_{sb} + \alpha^2 v_{sc}\right), \tag{14}$$

where $a = e^{j\frac{2\pi}{3}}$ is a unity vector. The last term in Eq. (13) equals zero according to the equation $\overline{\mathbf{V_{nN}}} = \frac{2}{3}v_{nN}\left(1 + \alpha + \alpha^2\right) = 0$. The voltage vector $\overline{\mathbf{V_{rN}}}$ in Eq. (13) can be defined as in the following equation:

$$\overline{\mathbf{V_{rN}}} = \overline{\mathbf{S_r}} \times V_{dc}, \tag{15}$$

where V_{dc} is the voltage of the DC link and $\overline{\mathbf{S_r}}$ represents the switching vector defined by the following expression:

$$\overline{\mathbf{S_r}} = \frac{2}{3}\left(S_1 + \alpha S_2 + \alpha^2 S_3\right) = S_{r\alpha} + jS_{r\beta}, \tag{16}$$

where S_i is defined as the state of phase i according to Eq. (17) and can take 0 , +1 , or –1 as its value based on the phase current polarity and the on/off state of the corresponding switch. As expressed in Eq. (18), T_i represents the on/off state for the switch of phase i and can take 1 or 0 as its value when the switch is on or off, respectively. It should be noted that when switch i is off, the corresponding phase current is not necessarily zero and it can flow through the diodes. The switching states of the rectifier can be obtained in the $\alpha\beta$ reference

frame as shown in Table 2 for an instant when the polarity of three phase currents is ($I_a > 0$, $I_b < 0$, $I_c < 0$). It should be noted that at each instant one vector is redundant and there are seven distinct vectors.

$$S_i = \begin{cases} 0 & T_i = 1 \\ +1 & T_i = 0 \text{ and } I_i > 0 \\ -1 & T_i = 0 \text{ and } I_i < 0; \end{cases} \tag{17}$$

$$T_i = \begin{cases} 0 & \text{switch i is off} \\ 1 & \text{switch i is on.} \end{cases} \tag{18}$$

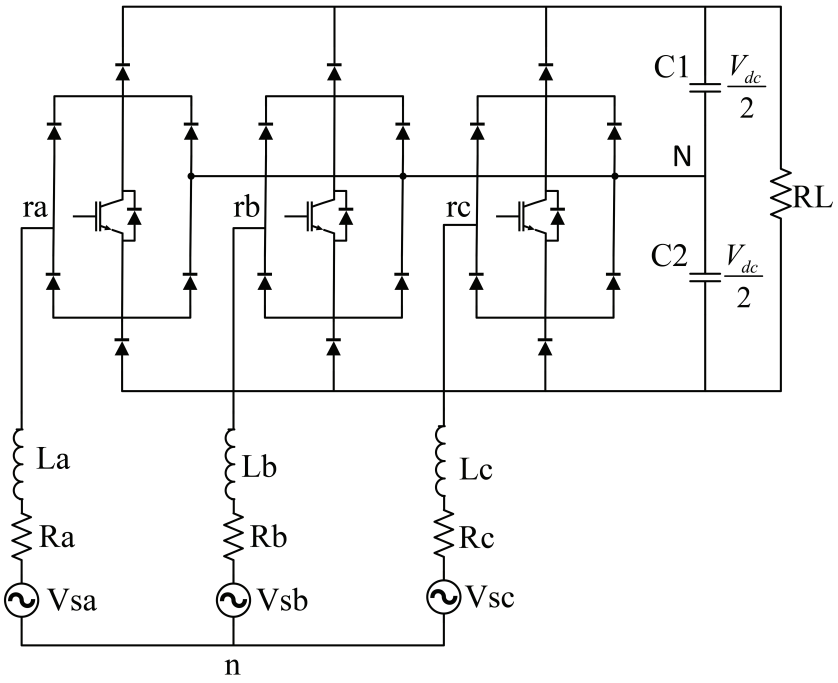

Figure 4. Vienna rectifier.

Table 2. Switching states and switching vectors.

T_1	T_2	T_3	S_1	S_2	S_3	$S_{r\alpha}$	$S_{r\beta}$
0	0	0	+1	-1	-1	$\frac{4}{3}$	0
0	0	1	+1	-1	0	1	$-\frac{\sqrt{3}}{3}$
0	1	0	+1	0	-1	1	$\frac{\sqrt{3}}{3}$
0	1	1	+1	0	0	$\frac{2}{3}$	0
1	0	0	0	-1	-1	$\frac{2}{3}$	0
1	0	1	0	-1	0	$\frac{1}{3}$	$-\frac{\sqrt{3}}{3}$
1	1	0	0	0	-1	$\frac{1}{3}$	$\frac{\sqrt{3}}{3}$
1	1	1	0	0	0	0	0

3. Proposed control scheme

The proposed control system includes an improved MPPT algorithm, which generates the speed reference corresponding to the optimal operating point. A simple and efficient technique is used to estimate the wind speed value. A multiobjective MPC strategy is designed and implemented for proper control of the Vienna converter with fast and accurate response and, at the same time, with minimum switching frequency. The different components of the designed control scheme will be discussed in this section.

3.1. Proposed MPPT algorithm

The proposed MPPT algorithm is designed in a way to eliminate the deficiencies of the conventional P&O algorithm by having fast and accurate tracking capability. In this algorithm, by having the estimated wind speed value, for which the estimation method will be discussed in the next subsection, the rotational speed reference is initially set to the value obtained from the following equation:

$$\omega_{ref0} = \frac{\lambda_{opt} V_w}{R}, \tag{19}$$

where V_w is the estimated wind speed. This speed reference is not precisely the optimal point because of the possible inaccuracies of wind speed estimation. Therefore, this point is called the pseudo-optimum operational point in this work, since it is close to the optimal point, but not exactly the same. After setting the operational point to the pseudo-optimum value, a small-step HCS search is employed to bring the operating point to the exact optimal point corresponding to the MPP. The basic principle of this strategy is depicted in Figure 5, where points P and O represent the pseudo-optimum and the exact optimum points, respectively. By utilizing this strategy, the HCS search needs much less time to track the MPP compared to the classical HCS method. This is because the algorithm begins the searching procedure from an initial point very close to the MPP. This algorithm has a high tracking speed, and the search step size can be chosen very small to reduce the oscillations around the MPP for achieving high accuracy, as well. Therefore, the proposed MPPT strategy is expected to have great tracking speed and accuracy.

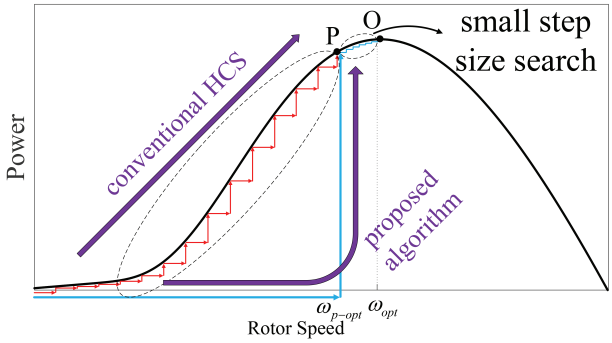

Figure 5. Basic principle of the proposed MPPT method.

Figure 6 shows the principle of the suggested MPPT method as a flowchart. If the algorithm detects that the wind speed has changed in three successive intervals, it considers this as a variation in the wind speed and will consequently update the initial point. Then the algorithm initiates a search procedure to find the exact optimal point. The flowchart of this part of the algorithm is depicted in Figure 7. After calculating the variations in the output power and rotational speed at each interval, the algorithm will decide to increase or

decrease the speed reference based upon the signs of these changes. Detection of the optimal point is checked after each step. This procedure will be repeated until the algorithm reaches the MPP. It should be noted that a simple and efficient check is used in this mode to ensure that the MPP is detected. The criterion in Eq. (20) ensures peak detection of the power-speed curve, which occurs when the MPPT has been accomplished:

$$\left|\frac{dp}{d\omega}\right| < \varepsilon, \tag{20}$$

where ε is a near-zero positive constant.

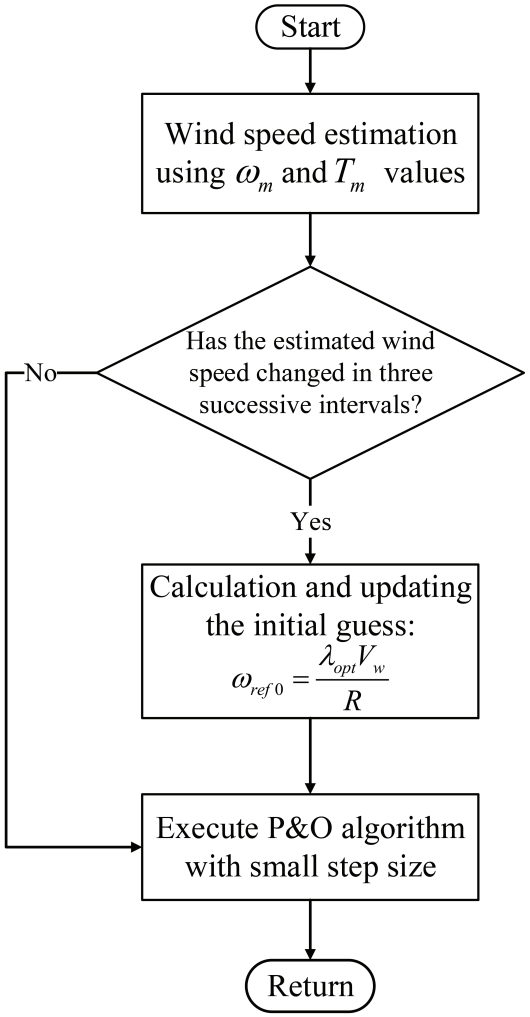

Figure 6. Simple flowchart of the proposed MPPT method.

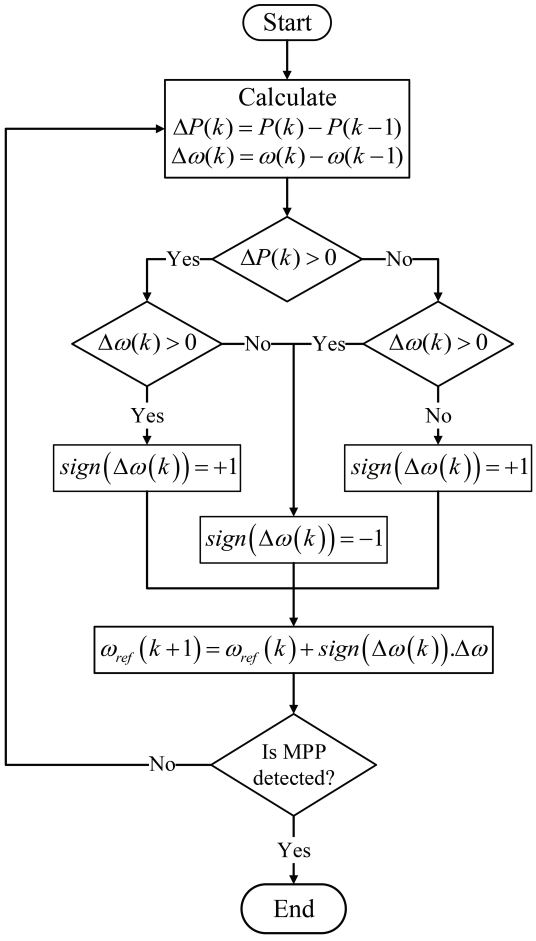

Figure 7. Search algorithm.

A general comparison is made between the proposed MPPT algorithm and the well-known conventional methods [6, 7] regarding different aspects and this is presented in Table 3.

Table 3. Comparison between the proposed MPPT algorithm and the conventional methods.

MPPT method	Convergence speed	Accuracy	Wind speed measurement	Prior training/ knowledge	Performance under varying wind speed
TSR	High	Low	Yes	Not required	Moderate
OTC & PSF	High	Low	No	Required	Moderate
P&O	Dependent on step size	Dependent on step size	No	Not required	Dependent on step size
Proposed	High	High	No	Not required	Good

3.1.1. Wind speed estimation

Measurement of the effective wind speed is one of the main issues in implementing MPPT algorithms in which wind speed value is required. Using wind speed sensors imposes great cost to the system and lowers the efficiency and reliability of the MPPT control algorithm. Moreover, the wind speed does not have the same value at different points around the swept area of the blades. The wind speed is measured using anemometers installed in some points on top of the nacelle. The measured values are the wind speed at those specific points and cannot represent the effective wind speed. Therefore, wind speed measurement does not have satisfactory accuracy [25]. Based on Eq. (1), the turbine mechanical torque can be written as expressed in the following equation:

$$T_m = \frac{P_m}{\omega_m} = \frac{1}{2}\rho\frac{c_p}{\omega_m}\pi R^2 {V_w}^3. \tag{21}$$

On the other hand, it was shown earlier that c_p can be represented by a polynomial function of λ according to Eq. (5). Moreover, according to Eq. (4) and by having the value of ω_m from measurements, λ is a function of wind speed V_w. Therefore, the estimation of the wind speed is accomplished by solving Eq. (22). The modified Newton–Raphson (MNR) algorithm [26] is used in this work to solve the estimation equation:

$$F(V_w) = T_m - \frac{1}{2}\rho\frac{c_p(\lambda)}{\omega_m}\pi R^2 {V_w}^3 \quad \text{where} \quad \lambda = \frac{R.\omega_m}{V_w}. \tag{22}$$

3.2. Predictive control of Vienna rectifier

The designed MPC controller for the Vienna rectifier is explained in this section. It should be mentioned that the modeling and equations for Vienna rectifier were presented earlier in Section 2.3. The first step is to obtain the prediction of the control variable (current vector) for the next sampling horizon ($\overline{\mathbf{I_s}}(k+1)$). In order to do so, the relation in Eq. (13) should be rewritten in discrete-time form. The current differentiation term $\frac{d}{dt}(\overline{\mathbf{I_s}})$ is discretized by the forward Euler approximation as given in Eq. (23):

$$\frac{d}{dt}(\overline{\mathbf{I_s}}) = \frac{\overline{\mathbf{I_s}}(k+1) - \overline{\mathbf{I_s}}(k)}{T_s}, \tag{23}$$

where T_s is the sampling time. According to the above explanation, the discrete-time form of Eq. (13) is given

in Eq. (24):

$$\overline{\mathbf{V_s}}(k) = L_s \frac{\overline{\mathbf{I_s}}(k+1) - \overline{\mathbf{I_s}}(k)}{T_s} + R_s \overline{\mathbf{I_s}}(k) + V_{dc} \overline{\mathbf{S_r}}(k). \tag{24}$$

By rearranging Eq. (24), the predicted current is obtained as expressed in Eq. (25):

$$\overline{\mathbf{I_s}}(k+1) = \frac{T_s}{L_s} \left[\overline{\mathbf{V_s}}(k) - V_{dc} \overline{\mathbf{S_r}}(k) \right] + \left(1 - \frac{T_s R_s}{L_s} \right) \overline{\mathbf{I_s}}(k). \tag{25}$$

In Eq. (25), every vector has two $\alpha\beta$ components by the general form of $\overline{X} = x_\alpha + j x_\beta$. Accordingly, the $\alpha\beta$ components of the predicted current vectors can be calculated using Eqs. (26) and (27):

$$i_{s\alpha}(k+1) = \frac{T_s}{L_s} \left[v_{s\alpha}(k) - V_{dc} S_{r\alpha}(k) \times \right] + \left(1 - \frac{T_s R_s}{L_s} \right) i_{s\alpha}(k), \tag{26}$$

$$i_{s\beta}(k+1) = \frac{T_s}{L_s} \left[v_{s\beta}(k) - V_{dc} S_{r\beta}(k) \times \right] + \left(1 - \frac{T_s R_s}{L_s} \right) i_{s\beta}(k). \tag{27}$$

In the designed MPC scheme, eight predicted current vectors $\overline{\mathbf{I_s}}(k+1)$ are calculated from Eq. (25) by using the measured currents and voltages $\overline{\mathbf{V_s}}(k)$, $\overline{\mathbf{I_s}}(k)$, and the eight selectable switching vectors. Then these predicted current vectors will be compared to the current reference $\overline{\mathbf{I_s^*}}(k+1)$ and the optimal actuation is determined based on minimizing the cost function. The cost function is defined in orthogonal coordinates as given in Eq. (28). The first two terms constitute the main part of it and ensure that the currents track their corresponding reference values. Another term is added to the cost function as a secondary objective to minimize the converter switching frequency, which directly corresponds to the switching loss. Limiting the switching frequency comes after the main objective of reference tracking in terms of importance and hence the third term is multiplied by the weighing factor μ:

$$g = \left[\left| i_{s\alpha}^* - i_{s\alpha} \right| + \left| i_{s\beta}^* - i_{s\beta} \right| \right] + \mu N_{sw}, \tag{28}$$

where $i_{s\alpha}^*$ and $i_{s\beta}^*$ are the real and imaginary parts of the reference current vector and $i_{s\alpha}$ and $i_{s\beta}$ are those for the predicted current vectors, respectively. N_{sw} is the number of switches whose statuses change in each iteration. The flowchart of the MPC method is shown in Figure 8, where x is a auxiliary variable for counting the eight possible switching states and evaluating the cost function for these states.

4. Simulation results

The studied system is modeled and simulated using the MATLAB/Simulink software package. The system parameters are given in Table 4. It is assumed that the studied WECS has resistive load. The performance of the proposed control scheme is studied for two different wind speed profiles. The first profile is depicted in Figure 9, in which the wind speed has step changes during the operation period. The proposed MPPT algorithm generates an optimal speed reference, which is depicted in Figure 10, plus the actual controlled value. It can be observed that the speed control has accurate performance. The power coefficient, mechanical power, and torque are depicted in Figures 11a, 11b, and 11c, respectively. The power coefficient in Figure 11a is constantly kept at its maximum value. When the wind speed suddenly changes, c_p drops for an instant, but the control

system immediately regulates it again to reach its maximum value. This supports the high speed and accuracy of the proposed control scheme in extracting the maximum power. The reference and actual values of the phase current are depicted in Figures 12a, 12b, and 12c. As can be seen in Figure 12c, because of utilizing the Vienna rectifier, and because of the advantages of the MPC-based scheme, the harmonic distortion in the current is very low and the currents have high-quality sinusoidal waveforms.

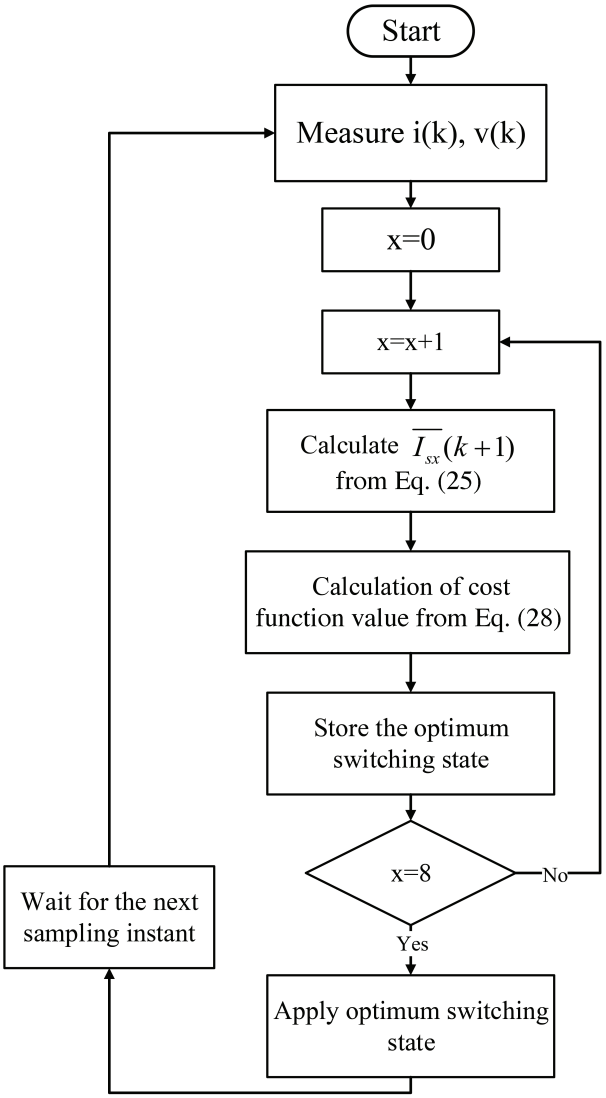

Figure 8. MPC flowchart.

In addition to the previous wind speed profile, another profile with rapid variations, which is closer to the reality of wind speed, is also considered to study the system performance. This profile is shown in Figure 13. The reference and actual values of rotational speed and the power coefficient are depicted in Figures 14 and 15, respectively. It can be seen that the power coefficient is constantly kept at its maximum value, which means that the maximum possible energy has been extracted from the wind during the whole operation period.

In order to compare the proposed method with the conventional P&O algorithm, the performance of the system using the P&O method with two different step sizes has been studied for the same wind speed profile.

Table 4. System parameters.

PMSG nominal power	5.2 kW
Base wind speed (v_{rated})	12 m/s
Maximum extracted power at v_{rated}	4 kW
Stator inductance ($L_d = L_q$)	1.67 mH
Stator resistance (R_s)	0.18 Ω
Permanent magnet flux	0.0714394 V s
PMSG inertia	0.0062 kg m^2e

For the first case, the generated speed reference by the P&O algorithm and the optimal speed corresponding to the MPP are shown in Figure 16. As can be seen in this figure, the P&O algorithm is slow and cannot keep up with the rapid variations in wind speed. Therefore, the rotational speed in this case has a delay in tracking the optimal value and there is a considerable difference between the actual rotor speed and the optimal value most of the time. This slow response of the P&O method affects the tracking of the optimal point and, as shown in Figure 17, the algorithm cannot properly keep the power coefficient at its maximum value and this will significantly reduce the extracted energy from wind and lower the system efficiency.

In another case, the step size of the P&O method is increased to make the algorithm faster and eliminate the delay in the previous case. Results similar to the previous case are shown in Figures 18 and 19. In this case, increasing the step size makes the algorithm fast enough to follow the wind speed variations, but it also causes unwanted oscillations in reference speed, which deteriorates the MPPT performance and reduces the accuracy and efficiency. The extracted energy during the operation period for the proposed algorithm and two cases of the P&O method are obtained for the same conditions by integrating the instant power over the operation time. These values are compared in Figure 20, which support the considerably higher efficiency of the proposed MPPT algorithm because it has extracted more energy from the wind.

In this part, the effect of the switching reduction term in the cost function is studied. This term was considered in the designed controller in order to minimize the switching frequency and consequently increase the converter efficiency. In order to verify this, the values of converter efficiency are compared in Figure 21 for two cases with and without this term in the cost function. As can be seen from this figure, adding this term has notably increased the converter efficiency, which verifies its advantageous effect.

Finally, a comparison is made between the current waveforms of the proposed method with a constant wind speed for two cases of using the Vienna rectifier and the bridge converter. The results are depicted in Figures 22a and 22b. It is clear that in the case of the Vienna rectifier, harmonic distortion is significantly lower and the current waveform has much higher quality. The total harmonic distortion (THD) value for the Vienna rectifier is 5.1% while it is 8.4% for the bridge rectifier.

5. Conclusion

In this article, a control scheme for a variable-speed PMSG-based standalone WECS has been proposed. The suggested algorithm improves the MPPT performance compared to the conventional P&O algorithm and eliminates the main challenge of trade-off between speed and accuracy. This algorithm has tracking speed and accuracy at the same time and, more importantly, it maintains this performance in the presence of rapidly varying wind speed. The Vienna rectifier is utilized in the designed system and has been controlled using a

multiobjective MPC-based controller. The results support the significant advantages of the proposed system and its superiority over conventional systems that use the P&O algorithm.

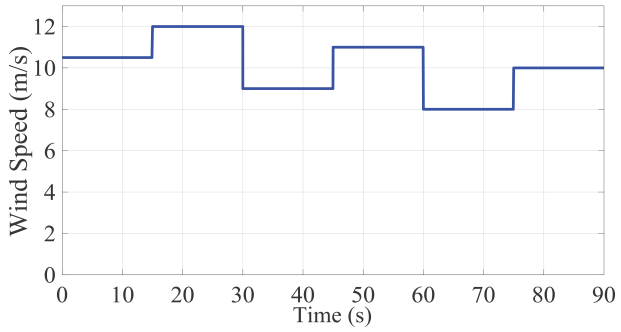

Figure 9. First wind speed profile.

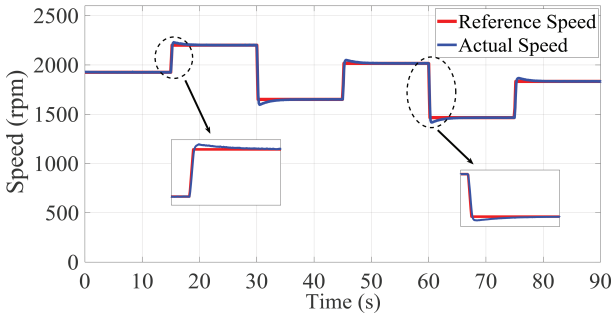

Figure 10. Rotational speed.

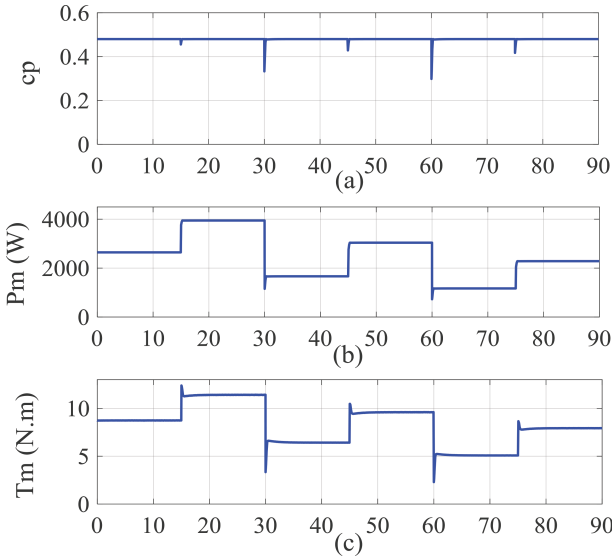

Figure 11. (a) Power coefficient, (b) mechanical power, (c) mechanical torque.

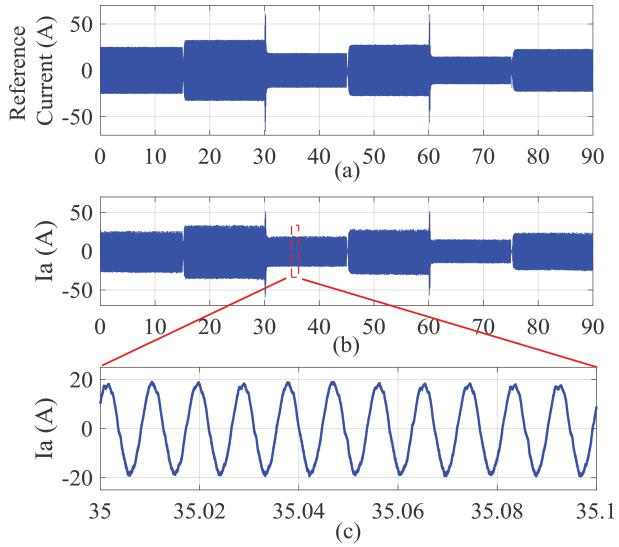

Figure 12. Phase current: (a) reference value, (b, c) actual value.

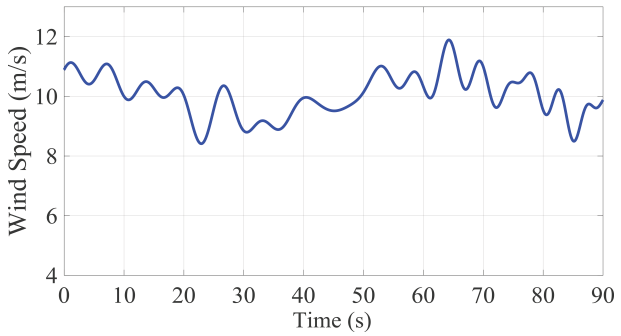

Figure 13. Second wind speed profile.

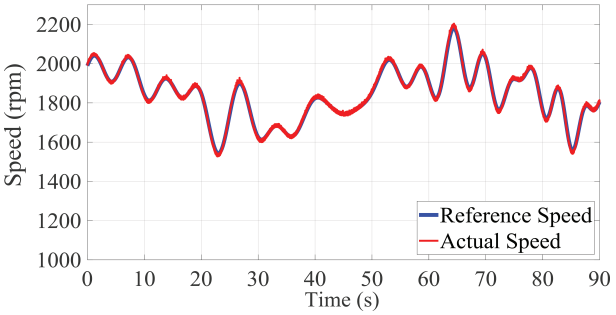

Figure 14. Rotational speed.

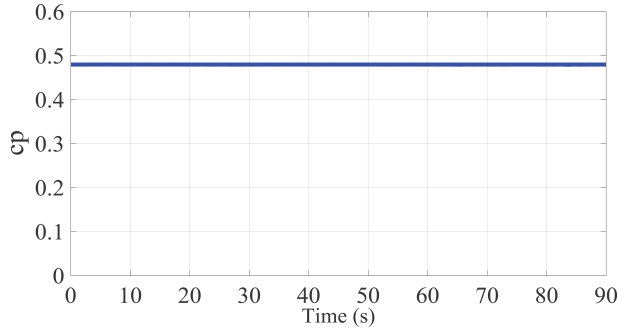

Figure 15. Power coefficient.

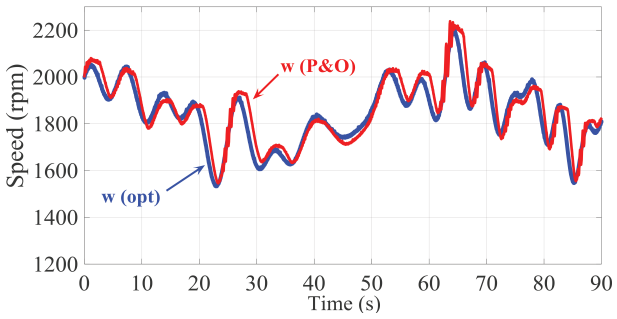

Figure 16. Rotational speed for P&O algorithm with small step size.

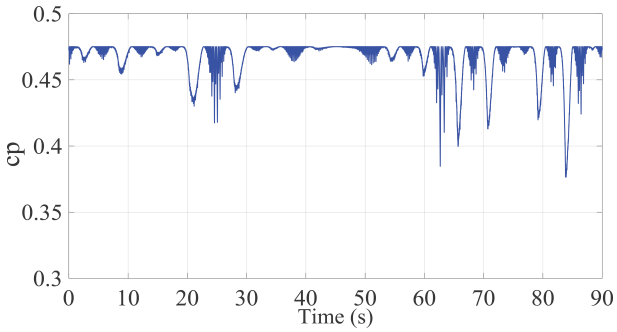

Figure 17. Power coefficient for P&O algorithm with small step size.

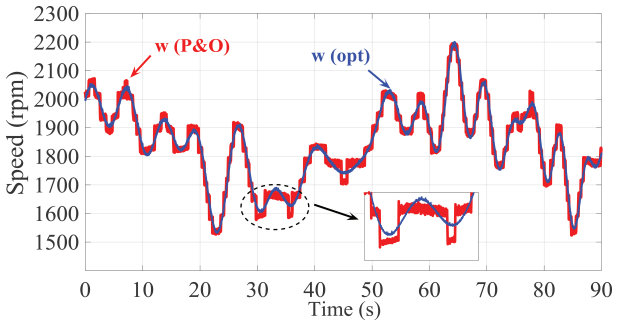

Figure 18. Rotational speed for P&O algorithm with large step size.

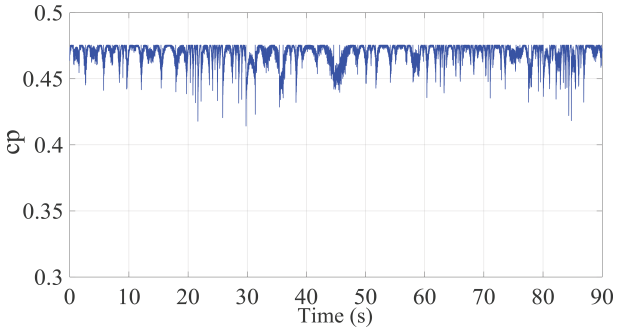

Figure 19. Power coefficient for P&O algorithm with large step size.

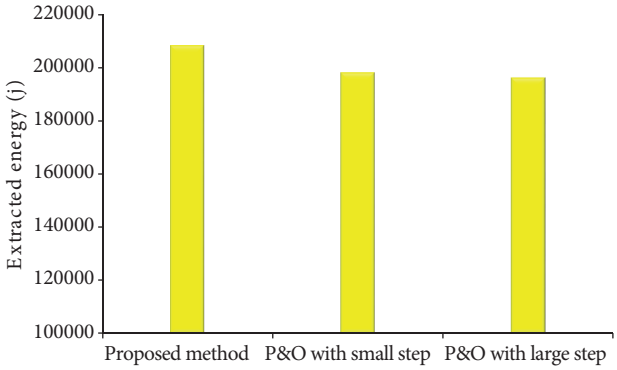

Figure 20. Comparison of extracted energy.

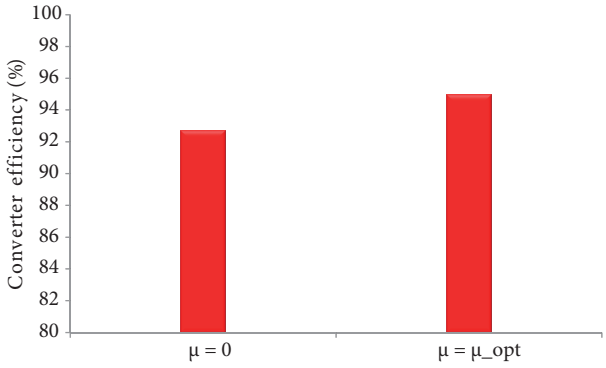

Figure 21. Comparison of converter efficiency.

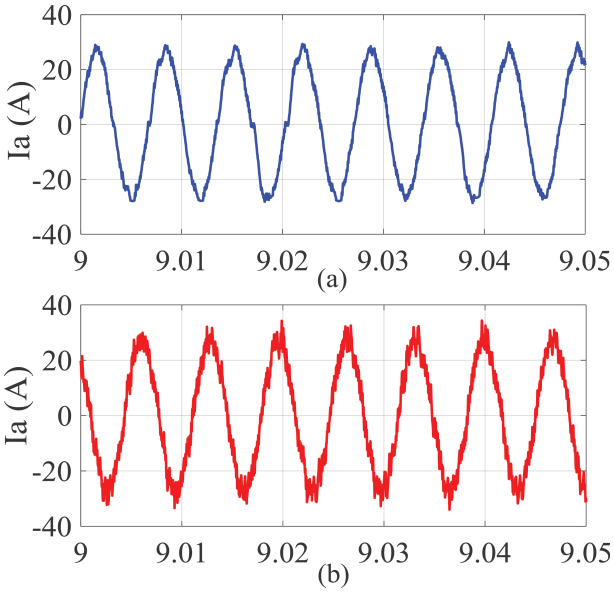

Figure 22. Phase current: (a) Vienna rectifier, (b) bridge rectifier.

References

[1] Zhao Y, Wei C, Zhang Z, Qiao W. A review on position/speed sensorless control for permanent-magnet synchronous machine-based wind energy conversion systems. IEEE Journal of Emerging and Selected Topics in Power Electronics 2013; 1 (4): 203-216. doi: 10.1109/JESTPE.2013.2280572

[2] de Freitas TR, Menegáz PJ, Simonetti DS. Rectifier topologies for permanent magnet synchronous generator on wind energy conversion systems: a review. Renewable and Sustainable Energy Reviews 2016; 54: 1334-1344. doi: 10.1016/j.rser.2015.10.112

[3] Kolar JW, Zach FC. A novel three-phase utility interface minimizing line current harmonics of high-power telecommunications rectifier modules. IEEE Transactions on Industrial Electronics 1997; 44 (4): 456-467. doi: 10.1109/41.605619

[4] Gadelovitz S, Kuperman A. Modeling and classical control of unidirectional Vienna rectifiers. In: 2012 Electric Power Quality and Supply Reliability; Tartu, Estonia; 2012. pp. 1-4.

[5] Rodriguez J, Cortes P. Predictive Control of Power Converters and Electrical Drives. Hoboken, NJ, USA: John Wiley & Sons, 2012.

[6] Kumar D, Chatterjee K. A review of conventional and advanced MPPT algorithms for wind energy systems. Renewable and Sustainable Energy Reviews 2016; 55: 957-970. doi: 10.1016/j.rser.2015.11.013

[7] Abdullah MA, Yatim AH, Tan CW, Saidur R. A review of maximum power point tracking algorithms for wind energy systems. Renewable and Sustainable Energy Reviews 2012; 16 (5): 3220-3227. doi: 10.1016/j.rser.2012.02.016

[8] Nasiri M, Milimonfared J, Fathi SH. Modeling, analysis and comparison of TSR and OTC methods for MPPT and power smoothing in permanent magnet synchronous generator-based wind turbines. Energy Conversion and Management 2014; 86: 892-900. doi: 10.1016/j.enconman.2014.06.055

[9] Li DY, Song YD, Gan ZX, Cai WC. Fault-tolerant optimal tip-speed-ratio tracking control of wind turbines subject to actuation failures. IEEE Transactions on Industrial Electronics 2015; 62 (12): 7513-7523. doi: 10.1109/TIE.2015.2458968

[10] Aubrée R, Auger F, Macé M, Loron L. Design of an efficient small wind-energy conversion system with an adaptive sensorless MPPT strategy. Renewable Energy 2016; 86: 280-291. doi: 10.1016/j.renene.2015.07.091

[11] Pagnini LC, Burlando M, Repetto MP. Experimental power curve of small-size wind turbines in turbulent urban environment. Applied Energy 2015; 154: 112-121. doi: 10.1016/j.apenergy.2015.04.117

[12] Uddin MN, Patel N. Maximum power point tracking control of IPMSG incorporating loss minimization and speed sensorless schemes for wind energy system. IEEE Transactions on Industry Applications 2016; 52 (2): 1902-1912. doi: 10.1109/TIA.2015.2510507

[13] Kesraoui M, Korichi N, Belkadi A. Maximum power point tracker of wind energy conversion system. Renewable Energy 2011; 36 (10): 2655-2662. doi: 10.1016/j.renene.2010.04.028

[14] Kazmi SM, Goto H, Guo HJ, Ichinokura O. A novel algorithm for fast and efficient speed-sensorless maximum power point tracking in wind energy conversion systems. IEEE Transactions on Industrial Electronics 2011; 58 (1): 29-36. doi: 10.1109/TIE.2010.2044732

[15] Du X, Yin H. MPPT control strategy of DFIG-based wind turbines using double steps hill climb searching algorithm. In: 2015 5th International Conference on Electric Utility Deregulation and Restructuring and Power Technologies; Changsha, China; 2015. pp. 1910-1914.

[16] Linus RM, Damodharan P. Wind velocity sensorless maximum power point tracking algorithm in grid-connected wind energy conversion system. Electric Power Components and Systems 2015; 43 (15): 1761-1770. doi: 10.1080/15325008.2015.1052158

[17] Rajaei AH, Mohamadian M, Dehghan SM, Yazdian A. PMSG-based variable speed wind energy conversion system using Vienna rectifier. European Transactions on Electrical Power 2011; 21 (1): 954-972. doi: 10.1002/etep.488

[18] Lee J, Kim YS. Sensorless fuzzy-logic-based maximum power point tracking control for a small-scale wind power generation systems with a switched-mode rectifier. IET Renewable Power Generation 2016; 10 (2): 194-202. doi: 10.1049/iet-rpg.2015.0250

[19] Yin XX, Lin YG, Li W, Liu HW, Gu YJ. Fuzzy-logic sliding-mode control strategy for extracting maximum wind power. IEEE Transactions on Energy Conversion 2015; 30 (4): 1267-1278. doi: 10.1109/TEC.2015.2422211

[20] Medjber A, Guessoum A, Belmili H, Mellit A. New neural network and fuzzy logic controllers to monitor maximum power for wind energy conversion system. Energy 2016; 106: 137-146. doi: 10.1016/j.energy.2016.03.026

[21] Wei C, Zhang Z, Qiao W, Qu L. An adaptive network-based reinforcement learning method for MPPT control of PMSG wind energy conversion systems. IEEE Transactions on Power Electronics 2016; 31 (11): 7837-7848. doi: 10.1109/TPEL.2016.2514370

[22] Mérida J, Aguilar LT, Dávila J. Analysis and synthesis of sliding mode control for large scale variable speed wind turbine for power optimization. Renewable Energy 2014; 71: 715-728. doi: 10.1016/j.renene.2014.06.030

[23] Heier S. Grid Integration of Wind Energy: Onshore and Offshore Conversion Systems. Hoboken, NJ, USA: John Wiley & Sons, 2014.

[24] Li S, Haskew TA, Xu L. Conventional and novel control designs for direct driven PMSG wind turbines. Electric Power Systems Research 2010; 80 (3): 328-338. doi: 10.1016/j.epsr.2009.09.016

[25] Jena D, Rajendran S. A review of estimation of effective wind speed based control of wind turbines. Renewable and Sustainable Energy Reviews 2015; 43: 1046-1062. doi: 10.1016/j.rser.2014.11.088

[26] Kreyszig E. Advanced Engineering Mathematics. Hoboken, NJ, USA: John Wiley & Sons, 1983.